A polymer canvas with the stiffness of the bone matrix to study and control mesenchymal stem cell response

Alessandra Zanut[a], Rui Li[a], Ru Deng[b], Xiangyu Liu[a], Martin Rejhon[a], Weiqiang Chen[a], Marcus Weck[b], Giuseppe Maria de Peppo[c], Elisa Riedo[a]**

Dr. Alessandra Zanut, Dr. Rui Li, Dr. Xiangyu Liu, Dr. Martin Rejhon, Prof. Weiqiang Chen, Prof. Elisa Riedo

Tandon School of Engineering, New York University

6 Metrotech, Brooklyn, NY 11201, United States
E-mail: elisa.riedo@nyu.edu

Prof. Marcus Weck, Dr. R Deng

Department of Chemistry, New York University

Silver Center Block, 100 Washington Square E, New York, NY 10003, United States

Dr. Giuseppe Maria de Peppo
The New York Stem Cell Foundation Research Institute

619 West 54th Street, New York, NY, 10019, United States

Mirimus, Inc

760 Parkside Ave, Brooklyn, NY 11226, United States

E-mail: gmd396@nyu.edu

Keywords: biomimicry, biomaterial, bone, extracellular matrix, induced mesenchymal stem cells, stiffness, polymer

Abstract

The possibility to reproduce *in vitro* the complex multiscale physical features present in the human tissues creates novel opportunities for biomedical advances and fundamental understanding of cell-environment interfaces and interactions. While stiffness has been recognized as a key property in influencing cell behavior, so far systematic studies on the role of stiffness have been limited to values in the KPa-MPa range, significantly below the stiffness of bone.

Here, we report a platform enabling the tuning and control of the stiffness of a biocompatible polymeric interface up to values characteristic of the bone tissue, which are in the GPa range. The ability to fine tune the stiffness up to these large values is achieved by using extremely thin polymer films on glass and cross-linking the films using UV light irradiation. We show that a higher stiffness is related to better adhesion, proliferation, and osteogenic differentiation, and that it is also possible to switch on/off cell attachment and growth by solely tuning the stiffness of the interface, without any surface chemistry or topography modification. Since the stiffness is tuned directly by UV irradiation, this platform is ideal for rapid and simple stiffness patterning, and stiffness gradients fabrication. This materials platform represents an innovative tool for combinatorial studies of the synergistic effect of tissue environmental cues on cell behavior, and creates new opportunities for next generation biosensors, single-cell patterning, and lab-on-a-chip devices.

1. Introduction

The last two decades have witnessed a large amount of research demonstrating that the mechanical properties of biological tissues play a fundamental role in controlling cell behavior[1]. In particular, tissue stiffness controls cell adhesion, migration, and proliferation, and acts as a strong driver for phenotypic commitment both *in vivo* and *in vitro*[2-5]. For example, atop soft hydrogels that mimic the stiffness of brain tissue, mesenchymal stem cells (MSCs) express neuronal biomarkers, whereas on rigid substrates they produce osteocalcin, a bone tissue-specific protein[4]. So far, most of the

investigations focused on understanding the effect of stiffness on cell behavior and differentiation rely on substrates having stiffness values ranging from kPa to a few MPa. These studies have been prevalently performed with collagen fibers and hydrogels pretreated with biologically relevant chemical functionalities[6-12]. On the other hand, studies using hard materials such as composites, ceramics, metals, and alloys suffer from the impossibility of tuning the stiffness while maintaining the same chemistry and/or topography[13-19]. Existing materials have therefore limited the ability to conduct systematic studies aimed at understanding the effect of bone tissue-compliant stiffness, i.e., 1 - 30 GPa, on cell behavior, independently from topography and chemistry.

Here, we demonstrate a novel and easy to implement methodology to study the effect of stiffness in a range of values typical of the bone tissues on adhesion, proliferation, and osteogenic differentiation of human MSCs. Our methodology is based on a cell culture compatible and quasi-atomically smooth polymer film, poly((tetrahydropyran-2-yl N-(2 methacryloxyethyl) carbamate)-b-(methyl 4-(3-methacryloyloxypropoxy) cinnamate)) (PMCC)[20,21], which has been demonstrated before to be topographically and chemically patternable with sub -10 nm precision[20-26]. We show that the stiffness of PMCC thin films can be tuned between 2 GPa and 28 GPa by cross-linking the polymer film using UV light irradiation. In this work, ultra-thin PMCC films are spin-coated on glass and irradiated with UV light for different exposure times, while the chemical and topographical properties are kept unaltered, as demonstrated by Fourier Transform Infrared (FTIR) spectroscopy and atomic force microscopy (AFM) characterization. To investigate the mechanical properties of the PMCC films, we perform AFM based nanoindentation experiments using colloidal probes showing a proportional increase of stiffness with UV exposure. To study the effect of stiffness on stem cell behavior, we culture MSCs derived from human induced pluripotent stem cells (iMSCs)[27] atop PMCC films of different stiffness, and investigate cell adhesion, morphology, and differentiation via

metabolic assay, microscopy, and staining of different cellular biomarkers. The results demonstrate that while iMSCs do not attach on untreated soft PMCC films, they grow on UV cross-linked films and show increased size, proliferation rate, and differentiation towards the bone lineage with increasing PMCC stiffness in the GPa range. In particular, we show that it is also possible to switch on/off cell attachment and growth by solely tuning the stiffness of the interface, without any surface chemistry or topography modification. The key role of stiffness in cell attachment and growth is also demonstrated by producing a PMCC polymer without cross-linkable cinnamate groups, which are responsible for the increase of polymer stiffness under UV treatment.

2. Results and Discussion

2.1 Crosslinking and characterization of PMCC samples

Figure 1a shows the chemical structure of the PMCC polymer[20,21] (more details in the experimental section), the key feature being the cinnamate groups that can be cross-linked by UV light exposure. In this study, PMCC was spin-coated on an Indium Tin Oxide (ITO) glass substrate to obtain thin films with a thickness between 25 and 40 nm. The cross-linking is performed in a UV oven using different exposure times, i.e., 1, 2, 4, and 8 hours, as described in the experimental section. Figure 1b and 1c present the FTIR spectra of PMCC films exposed to UV light (245 nm) for 0-8 hours. The results demonstrate the gradual disappearance of the peaks associated with the double bond stretching mode of the cinnamate group (~1600 cm^{-1}), indicating an increasing rate of cross-linking associated with increasing UV exposure. Furthermore, the spectra show that no other chemical changes are observed during the UV irradiation-based cross-linking step. To study the stiffness of such thin films, we adopted an atomic force microscopy nanoindentation method with a colloidal probe[28], which allows indentations of about 2 nm (see Supporting Information, Table S1), and therefore provides the elastic modulus of the polymer films independently from the underneath substrate. Figure 1d

shows the experimental nanoindentation curves where the force required to indent a spherical colloidal probe into the films is plotted against the corresponding indentation depth for a glass substrate, for a PMCC film non treated by UV light, and for PMCC films exposed to UV light for 1, 2, 4, and 8 hours. The values of the Young's moduli are obtained from the Hertzian fitting[29] of the indentation curves (see experimental section) and are reported in Fig. 1e. These values indicate that PMCC films with increasing cross-linking display higher Young's moduli. In particular, the Young's modulus grows from about 2 GPa for the non-UV treated samples to 28 GPa for the sample treated for 8 hours, whereas the Young's modulus of glass is 48 GPa.

2.2 Cell growth on PMCC samples

In Figure 2, we present cell studies where human iMSCs are cultured on PMCC films before and after UV treatment for 1, 2, 4, and 8 hours. Importantly, light micrographs (Figure 2a-e), taken after 5 days of culture, reveal that cells do not attach and grow on PMCC films untreated with UV light (having a stiffness of 2 GPa), while they attach and proliferate increasingly better on PMCC films with an increasingly higher degree of cross-linking and stiffness (corresponding to longer UV treatments). This behavior might result from the fact that cells form a higher number of focal adhesions atop the polymer mesh following cross-linking, and therefore attach stronger to the UV treated samples. Presto blue analysis, which measures the metabolic activity of the cells and is a good indicator of cell proliferation, further demonstrates the significant increase in growth potential shown by cells cultured on PMCC films treated with UV light for longer periods of time. The capability to switch on and off cell attachment on a film, as well as to create cell attachment gradients by simple and direct UV light exposure creates exciting possibilities for fast and easy single-cell patterning, cell circuitry

for cell-cell interaction studies, and tissue junctions for regenerative medicine applications. Indeed, we show that it is possible to localize cells only in the areas of the PMCC polymer which are exposed to UV light (Figure 2g-h), leaving the untreated regions clear of cells.

To demonstrate that the UV treatment increases the stiffness of the PMCC polymer through cross-linking, we design an *ad-hoc* experiment and produce a new polymer with the same chemical composition of PMCC but lacking the cross-linking cinnamate groups. We then expose these new PMCC films to UV light and compare FTIR spectra and cell behavior on these films with those having the cinnamate groups (see Figure 3). FTIR spectra prove that the band related to the double bond stretching mode of the cinnamate group at around 1600 cm^{-1} (as observed in Figure 1c and d for non-UV treated PMCC films) is not present in the cinnamate-free PMCC films, for both the UV treated and untreated samples (Figure 3a pink and purple spectra, respectively). On the other hand, as already discussed in Figure 1, the UV treatment of the PMCC films containing the cinnamate moieties activates the cross-linking process, such that the double bond stretching mode disappears in the FTIR spectra. The cell culture studies show that the UV treatment is effective to switch on cell attachment and proliferation only when the PMCC contains the cross-linkable cinnamate groups (Figure 3c), indicating that the stiffness is indeed the only property responsible for this behavior. Fig 3b shows that cells seeded on the cinnamate-free PMCC films do not attach and/or do not grow. Finally, we investigated the roughness and contact angle of the regular and cinnamate-free PMCC films with and without UV treatment (Figure S1). We found that the roughness is always very low (below 1 nm over 1 μm^2) for all samples, whereas a small increase in contact angle is observable after UV treatment in films with and without cinnamate groups. However, these changes are not responsible for the differences in cell attachment and growth observed after UV treatment, because they are similar in the films with and without cinnamate groups.

2.3 Cell size and adhesion on PMCC samples with increasing stiffness

Several studies have shown that substrate stiffness can control cell behavior, and act as a strong driver for phenotypic commitment *in vitro*[1]. Many studies have also shown that the substrate stiffness can be tuned *ad-hoc* to control cell morphology and adhesion, however, in these investigations the stiffness of the substrates was low and ranged between KPa and a few MPa[6-11]. This has hindered systematic studies aimed at understanding the effects of bone tissue-compliant stiffnesses, which are in the GPa range[30,31], on adhesion, migration, proliferation, and differentiation of human stem cells. Furthermore, these studies have been prevalently performed with collagen fibers and hydrogels pretreated with biologically relevant functionalities[12,32,33], making it difficult to distinguish the effects of chemistry, topography, and stiffness alone. Above here we have shown the possibility to tune the stiffness of an atomically smooth substrate in the range of the cortical bone stiffness, i.e., GPa range, while keeping the chemistry and topography unaltered. In Figure 4a, confocal microscopy images of human iMSCs after 1 week of culture on PMCC films cross-linked for 1, 2, 4, and 8 hours are presented. The results show that cells are significantly larger when cultured on PMCC films with higher stiffness, with cell areas about six times larger when cultured on PMCC films treated with UV light for 8 hours compared to samples treated for 1 hour. In addition, cells cultured on stiffer PMCC films display a spread flattened morphology, characterized by a different arrangement of the cytoskeleton, as observed by a change in the distribution of F-actin microfilaments, becoming more similar to osteoblastic cells[34-36]. Furthermore, cells cultured on PMCC films with increasing values of stiffness feature a significant increase in focal adhesions per cell, as evidenced by a five-fold increase in the number of vinculin patches per cell and more than a three-fold increase in focal adhesion kinase (FAK) intensity observed from 1 to 8 hours treatment with UV light (Figure 4b). These biomarkers are central mediators for mechanosensing and their increased production on stiffer PMCC films is responsible for the observed enhanced cell

attachment, larger cell size, and osteoblastic-like morphology on films UV treated for longer periods of time[37].

2.4 Osteogenic differentiation

Substrate stiffness also influences the differentiation ability of stem cells[1], with increasing stiffnesses promoting differentiation toward tissue characterized by higher Young's modulus. In Figure 5a, we present confocal microscopy images of human iMSCs after 2 weeks of culture on PMCC films cross-linked for 1, 2, 4, and 8 hours. In the nucleus, runt-related transcription factor-2 (RUNX2) regulates the expression of downstream genes involved in bone development, including genes encoding for the bone-related proteins alkaline phosphatase (ALP), osteocalcin (OC), and osteopontin (OPN), which are involved in bone metabolism and mineralization[27,38-41]. The results in Figure 5 show a significant higher localization of RUNX2 in the nucleus (see dashed red circular lines) when cells are cultured on PMCC films with 28 GPa stiffness compared to softer films. In consequence, Figure 5b also shows that the increased in stiffness leads to a significant increase in the production of the bone-specific proteins osteocalcin and osteopontin. Fluorescence data are confirmed by RT-qPCR analysis (Figure 6), displaying increased expression of the osteogenic genes RUNX2, ALP, and OPN 2 weeks after culture in osteogenic medium. Interestingly, the data show that cells cultured on tissue culture polystyrene (TCP) express higher RUNX2 and ALP and less OPN than cells cultured on PMCC samples after 2 weeks of culture in osteogenic medium, indicating PMCC samples promote differentiation more efficiently. Since TCP is softer than all the PMCC samples, the results support the idea that substrate stiffness promotes osteogenic differentiation also in the GPa range (i.e., 19 GPa to 28 GPa), as opposite to previous research showing that osteoblastic differentiation of stem cells is mainly controlled in the kPa – MPa stiffness range[6-11].

3. Conclusion

In this study, we report a simple and fast method to tune and control the stiffness of a biocompatible polymeric interface up to the values characteristic of the bone tissue, and we demonstrate the impact of GPa range stiffness on stem cell attachment, growth, and differentiation. The ability to fine tune the stiffness up to 30 GPa is achieved by using extremely thin polymer films on glass, and UV cross-linking. We demonstrate that not only a higher stiffness is related to better attachment, proliferation, and bone differentiation, but it is also possible to switch on/off cell attachment and growth by tuning the stiffness of the interface, without any surface chemistry or topography modification. The capability to switch on and off cell attachment on a film, as well as to create cell attachment gradients by simple and direct UV light exposure creates exciting possibilities for fast and easy single-cell patterning and cell-cell interaction studies, as well as for conducting durotaxis studies and engineering the gradual variation of stiffness typical of interface tissues such as the osteotendinous tissue junction.

Finally, we remark that the here discussed PMCC biocompatible polymer is a thermosensitive polymer used as resist in thermal scanning probe lithography, and therefore it can also be topographically and chemically patterned with any desired quasi-3D topography with sub-10 nm resolution, as shown in previous studies[21,22,26]. This platform is thus a white canvas for cells studies, where individual environmental cues, i.e., substrate topography, chemistry, and mechanical properties, can be tuned to study their individual and synergistic effect on cell behavior. It also creates new opportunities for next generation biosensors and lab-on-a-chip devices.

4. Experimental Section

4.1 Substrate and PMCC film preparation

ITO-coated glasses (1 cm x 1 cm) with a thickness of 1.1 mm (MSE Supplies, LLC, Tucson, AZ) were cleaned by ultrasonication in acetone, methanol, and isopropanol alcohol for 3 minutes each. Samples were treated with O_2 plasma for 30 minutes to increase adhesion and remove organic residuals on the surface. Then, the PMCC resist was dissolved in cyclohexanone (10 mg/ml) and spin-coated on the ITO glasses at 1500 rotation per minute for 60 seconds in a clean room environment. Afterwards, the samples were baked on a hot plate at 50°C for 10 minutes to remove residual solvent. The resulting film thickness ranges from 24 to 36 nm. The film preparation conditions and properties have been previously optimized to achieve high adhesion to the substrate, stability and biocompatibility[21]. In this study, polymer films have been exposed to UV light at 245 nm for 1, 2, 4, and 8 hours to cross-link the cinnamate moieties of the PMCC resist using a CL-1000 ultraviolet crosslinker (UVP®) with an energy of 999 x 100 µJ/cm^2.

4.2 Atomic Force Microscopy

Thickness and roughness of the PMCC films were studied on a Bruker MultiMode 8 AFM using tapping mode imaging. Flattening and z-scale adjustment of AFM images were performed with the Gwyddion software. Surface roughness was measured by scanning different areas of 1 x 1 µm. Final values were calculated by the average of 4 different areas.

4.3 AFM NanoIndentation

We determined the Young's moduli (E) of the PMCC films via AFM – nanoindentation using a Bruker MultiMode 8 AFM. A detailed description of the method is extensively reported in Ref[28,42]. All measurements were carried out in open air using a colloidal AFM probe with 1µm diameter

(Novascan Technologies, USA). Colloidal probes were calibrated with a NanoScope V controller using the thermal noise method[43]. Prior to the measurements, we calibrated the cantilever deflection sensitivity on a bare ITO/glass sample. Afterwards, force-distance curves were obtained with a constant approach velocity of 0.1 Hertz, while the indentation depth was varied from 1.22 to 2.17 nm (Table S1). For better statistics, we acquired force distance curves on 4 different regions for each investigated sample. On each region an area of 5 x 5 um^2 was selected, and nanoindentation measurements were performed on a matrix of 25 points in total (100 points for each sample). The Young's moduli E of the samples were extracted from the force-distance curves by fitting via the nonlinear Hertz's model[29]:

$$F_N = \frac{4E\sqrt{R_{tip}}}{3} z_{indent}^{3/2},$$

where F_N is the applied load, R_{tip} is the tip radius and z_{indent} is the indentation depth. The listed Young's moduli in Figure 1e were obtained as average values from all performed measurements together with the corresponding standard deviation.

4.4 Fourier Transform Infrared spectroscopy

FT-IR spectra of the PMCC films were recorded in the range of 4000–1000 cm^{-1} on a Nicolet 6700 FTIR spectrophotometer (Thermo Fisher, USA) using an ZnSe Polished Parallelogram ATR Prisms (50 x 10 x 1 mm) with a spectral resolution of 4 cm^{-1} and averaging on 100 scans.

Aliquots of PMCC resist with a concentration of 10 mg/ml (w/v) were drop-casted on the ZnSe prism substrate, previously treated with O_2 plasma for 30 minutes, and baked on a hot plate at 50°C for 10 minutes to remove the residual solvent. PMCC films were then exposed to UV light at 245 nm for 1,

2, 4, and 8 hours. The PMCC spectra were obtained by subtraction of a baseline consisting of the bare ZnSe substrate spectrum recorded in the same range.

4.5 Cell culture

Human iMSCs were derived and characterized as previously described[5,44]. For all studies, aliquots of cell suspension were seeded to the PMCC-coated ITO glasses placed in ultra-low attachment plates (Fisher Scientific) at a density of ~1,000 - 10,000 cells cm^{-2}. To study attachment and proliferation, cells were cultured in expansion medium, consisting of high-glucose KnockOut Dulbecco's modified Eagle's medium (DMEM; Gibco) supplemented with 20% (v/v) HyClone™ fetal bovine serum (FBS; GE Healthcare Life Sciences), beta-fibroblast growth factor (1 ng/mL; Invitrogen), nonessential amino acids (0.1 mM; Gibco), GlutaMAX (2 mM; Gibco), beta-mercaptoethanol (0.1 mM; Gibco), and antibiotic-antimycotic (100 U/mL; Gibco), while to study osteogenic differentiation cells were cultured in the commercially available OsteoLife™ Complete Osteogenesis Medium (Lifeline Cell Technologies). Following cell seeding, samples were placed in a humidified environment at 37°C for 5 hours to let cells attach, and then cultured in either expansion or osteogenic media for up to 14 days. Media were changed every 2-3 days. Cell seeding, attachment, and growth were monitored using the EVOS® FL Cell Imaging System (Life Technologies).

4.6 PrestoBlue assay

The metabolic activity of cells cultured on UV treated and untreated PMCC films was studied as an index of cell growth using the PrestoBlue™ reagent (Life Technologies). Briefly, samples were treated with 1 ml of expansion medium containing 10% (v/v) of PrestoBlue™ reagent (Life Technologies), and

incubated for 1 hour at 37°C. Following incubation, 200 µl aliquots of culture media were transferred to a black, clear, flat-bottom 96-well plate (BD Falcon™), and fluorescence measured at 560/590 nm (excitation/emission) using the fluorescent reader SYNERGYMx (BioTek) equipped with the Gen 5 1.09 software.

4.7 Cell painting

Cells were stained to study adhesion, morphology, and differentiation toward the osteogenic lineage. To study cell adhesion and morphology, cells cultured in expansion medium for 1 week (see above) were washed three times with Dulbecco's phosphate buffer saline solution (DPBS; Gibco) and then fixed using a 4% (v/v) paraformaldehyde solution in DPBS (Chem Cruz®, Santa Cruz) for 15 minutes. After washing, cells were permeabilized with 0.25% TritonX-100 in DPBS for 30 minutes at room temperature, then blocked with 3% (w/v) bovine serum albumin (BSA) in DPBS for 60 min at 37 °C.

For staining focal adhesions, Alexa Fluor 488 anti-Vinculin antibody (ab196454, 1:500, Abcam) and anti-FAK antibody (610087, 1:200, BD Biosciences) were used. For staining osteogenic biomarkers, anti-RUNX2 antibody (NBP1-77461, 1:500, NOVUS Biologicals), anti-osteocalcin antibody (MAB1419, 1:100, R&D Systems), and eFluor™ 660 anti-osteopontin antibody (50-9096-42, 1:50, Thermo Fisher Scientific) were used. All solutions containing primary antibodies were prepared in 1% (w/v) BSA. Afterwards, samples were thoroughly washed with PBS and incubated with staining solution containing the secondary antibodies Alexa Fluor 647 goat anti-mouse (A32728, 1:1000, Invitrogen), Alexa Fluor 555 goat anti-mouse (A-21422, 1:1000, Invitrogen), DyLight™ 488 donkey anti-rabbit (SA5-10038, 1:500, Invitrogen), and Alexa Fluor 555 phalloidin (0.33uM, 8953S, Cell Signaling

Technology) for two hours at room temperature. Nuclei were counterstained with DAPI (1:1000, 62248, Thermo Scientific) for 30 minutes at 37 °C. After staining, samples were mounted on the coverslips and imaged with a Nikon C2 confocal microscopy (Nikon, Japan).

Fluorescent images of cells cultured on different PMCC films were quantified using the ImageJ software (National Institutes of Health, Baltimore, Maryland, USA). Fluorescent images were converted to 8-bit grayscale images to select cell boundaries based on the actin or osteocalcin staining. Following, cell ranges were saved as regions of interest, and the fluorescent intensity of these regions was measured for each stained biomarker in twenty cells from each group. Results were acquired from three independent experiments. The quantify the number of vinculin patches in each cell the "Binary" and the "Analyze Particles" functions in ImageJ were used.

4.8 Real-time quantitative polymerase chain reaction

Expression of osteogenic genes was measured via RT-qPCR. Briefly, 2 weeks after culture in osteogenic medium, cells were washed 3 times with PBS and lysed with 350 µL of RLT buffer (QIAGEN). RNA was extracted from cell lysates with a Quick-RNA Miniprep Plus isolation kit (Zymo Research) according to the manufacturer's protocol, and concentration measured with a NanoDrop One spectrophotometer (NanoDrop Technologies). Following, 1 µg of RNA per each sample was reverse transcribed into cDNA using the RevertAid First Strand cDNA Synthesis Kit (Thermo Fisher Scientific), and qPCR was run using the CFX96 touchreal-time PCR detection mix reagent (Thermo Fisher Scientific) and primers (GENEWIZ; Table S2) specific for runt-related transcription factor 2 (RUNX2), alkaline phosphatase (ALP), osteopontin (OPN), and the housekeeping gene glyceraldehyde 3-phosphate dehydrogenase (GAPDH). The expression levels of osteogenic genes were normalized to the respective expression levels of GAPDH and calculated with the $2^{-\Delta\Delta Ct}$ method.

4.9 Statistical analysis

Statistical analysis was conducted using Prism 9 (GraphPad). One-way ANOVA followed by Tukey's multiple comparisons test was used to assess significant differences between groups. All results are shown as means and ± standard deviations. Differences were considered statistically significant when the p value was less than 0.05.

Acknowledgments

This work was supported by the U.S. Department of Energy, Office of Science, Basic Energy Sciences, MSE Division under Award # DE-SC0018924, the US Army Research Office under Award # W911NF2020116, the NSF CBET grant # 1914539, and the NSF MRSEC at NYU. We thank the Global Stem Cell Array® team at NYSCF for providing the human iPSC line. Funding for GMdP was provided by The New York Stem Cell Foundation Research Institute, and the Ralph and Ricky Lauren Family Foundation.

References

1 Guimaraes, C. F., Gasperini, L., Marques, A. P. & Reis, R. L. The stiffness of living tissues and its implications for tissue engineering. *Nat Rev Mater* **5**, 351-370, doi:10.1038/s41578-019-0169-1 (2020).

2 Tse, J. R. & Engler, A. J. Stiffness gradients mimicking in vivo tissue variation regulate mesenchymal stem cell fate. *PLoS One* **6**, e15978, doi:10.1371/journal.pone.0015978 (2011).

3 Vazquez, C. P. *et al.* Variation of polyelectrolyte film stiffness by photo-cross-linking: a new way to control cell adhesion. *Langmuir* **25**, 3556-3563, doi:10.1021/la803577t (2009).

4 Engler, A. J., Sen, S., Sweeney, H. L. & Discher, D. E. Matrix elasticity directs stem cell lineage specification. *Cell* **126**, 677-689, doi:10.1016/j.cell.2006.06.044 (2006).

5 Gultian, K. A. *et al.* Human induced mesenchymal stem cells display increased sensitivity to matrix stiffness. *Scientific Reports* **12**, 8483, doi:10.1038/s41598-022-12143-2 (2022).

6 Chen, L. *et al.* Biomimetic mineralized microenvironment stiffness regulated BMSCs osteogenic differentiation through cytoskeleton mediated mechanical signaling transduction. *Mater Sci Eng C Mater Biol Appl* **119**, 111613, doi:10.1016/j.msec.2020.111613 (2021).

7 Hou, Y. *et al.* Surface Roughness and Substrate Stiffness Synergize To Drive Cellular Mechanoresponse. *Nano Lett* **20**, 748-757, doi:10.1021/acs.nanolett.9b04761 (2020).

8 Jin, R. *et al.* Biomineralization and osteogenic differentiation modulated by substrate stiffness. *European Polymer Journal* **122**, doi:10.1016/j.eurpolymj.2019.109395 (2020).

9 Lee, H. S. *et al.* Engineered Phage Matrix Stiffness-Modulating Osteogenic Differentiation. *ACS Appl Mater Interfaces* **10**, 4349-4358, doi:10.1021/acsami.7b17871 (2018).

10 Sun, M. *et al.* Extracellular matrix stiffness controls osteogenic differentiation of mesenchymal stem cells mediated by integrin alpha5. *Stem Cell Res Ther* **9**, 52, doi:10.1186/s13287-018-0798-0 (2018).

11 Wan, W. *et al.* Synergistic Effect of Matrix Stiffness and Inflammatory Factors on Osteogenic Differentiation of MSC. *Biophys J* **117**, 129-142, doi:10.1016/j.bpj.2019.05.019 (2019).

12 Xu, L. *et al.* An injectable gellan gum-based hydrogel that inhibits Staphylococcus aureus for infected bone defect repair. *J Mater Chem B* **10**, 282-292, doi:10.1039/d1tb02230j (2022).

13 Gao, C., Peng, S., Feng, P. & Shuai, C. Bone biomaterials and interactions with stem cells. *Bone Res* **5**, 17059, doi:10.1038/boneres.2017.59 (2017).

14 Metavarayuth, K., Sitasuwan, P., Zhao, X., Lin, Y. & Wang, Q. Influence of Surface Topographical Cues on the Differentiation of Mesenchymal Stem Cells in Vitro. *Acs Biomater Sci Eng* **2**, 142-151, doi:10.1021/acsbiomaterials.5b00377 (2016).

15 Dalby, M. J. *et al.* The control of human mesenchymal cell differentiation using nanoscale symmetry and disorder. *Nat Mater* **6**, 997-1003, doi:10.1038/nmat2013 (2007).

16 Aravamudhan, A. *et al.* Collagen nanofibril self-assembly on a natural polymeric material for the osteoinduction of stem cells in vitro and biocompatibility in vivo. *Rsc Adv* **6**, 80851-80866, doi:10.1039/c6ra15363a (2016).

17 Friguglietti, J. *et al.* Novel silicon titanium diboride micropatterned substrates for cellular patterning. *Biomaterials* **244**, 119927 (2020).

18 Kavand, H. *et al.* Cell-imprint surface modification by contact photolithography-based approaches: Direct-cell photolithography and optical soft lithography using PDMS cell imprints. *ACS applied materials & interfaces* **11**, 10559-10566 (2019).

19 Li, J. *et al.* Repair of infected bone defect with Clindamycin-Tetrahedral DNA nanostructure Complex-loaded 3D bioprinted hybrid scaffold. *Chemical Engineering Journal* **435**, 134855, doi:https://doi.org/10.1016/j.cej.2022.134855 (2022).

20 Wang, D. B. *et al.* Thermochemical Nanolithography of Multifunctional a Nanotemplates for Assembling Nano-objects. *Adv Funct Mater* **19**, 3696-3702, doi:10.1002/adfm.200901057 (2009).

21 Liu, X. *et al.* Cost and Time Effective Lithography of Reusable Millimeter Size Bone Tissue Replicas With Sub-15 nm Feature Size on A Biocompatible Polymer. *Adv Funct Mater* **31**, 2008662 (2021).

22 Liu, X. *et al.* Sub-10 nm Resolution Patterning of Pockets for Enzyme Immobilization with Independent Density and Quasi-3D Topography Control. *ACS Appl Mater Interfaces* **11**, 41780-41790, doi:10.1021/acsami.9b11844 (2019).

23 Albisetti, E. *et al.* Thermochemical scanning probe lithography of protein gradients at the nanoscale. *Nanotechnology* **27**, 315302 (2016).

24 Carroll, K. M. *et al.* Fabricating nanoscale chemical gradients with thermochemical nanolithography. *Langmuir* **29**, 8675-8682 (2013).

25 Wang, D. *et al.* Thermochemical Nanolithography of Multifunctional Nanotemplates for Assembling Nano-Objects. *Adv Funct Mater* **19**, 3696-3702 (2009).

26 Albisetti, E. *et al.* Thermal scanning probe lithography. *Nature Reviews Methods Primers* **2**, doi:10.1038/s43586-022-00110-0 (2022).

27 de Peppo, G. M. *et al.* Engineering bone tissue substitutes from human induced pluripotent stem cells. *Proc Natl Acad Sci U S A* **110**, 8680-8685, doi:10.1073/pnas.1301190110 (2013).

28 Carl, P. & Schillers, H. Elasticity measurement of living cells with an atomic force microscope: data acquisition and processing. *Pflugers Arch* **457**, 551-559, doi:10.1007/s00424-008-0524-3 (2008).

29 Derjaguin, B. V., Muller, V. M. & Toporov, Y. P. Effect of contact deformations on the adhesion of particles. *Journal of Colloid and interface science* **53**, 314-326 (1975).

30 Rho, J. Y., Ashman, R. B. & Turner, C. H. Young's modulus of trabecular and cortical bone material: ultrasonic and microtensile measurements. *J Biomech* **26**, 111-119, doi:10.1016/0021-9290(93)90042-d (1993).

31 Morgan, E. F., Unnikrisnan, G. U. & Hussein, A. I. Bone Mechanical Properties in Healthy and Diseased States. *Annu Rev Biomed Eng* **20**, 119-143, doi:10.1146/annurev-bioeng-062117-121139 (2018).

32 Zhang, T. *et al.* Myelosuppression Alleviation and Hematopoietic Regeneration by Tetrahedral-Framework Nucleic-Acid Nanostructures Functionalized with Osteogenic Growth Peptide. *Advanced Science*, 2202058 (2022).

33 Li, S. *et al.* Bioswitchable delivery of microRNA by framework nucleic acids: application to bone regeneration. *Small* **17**, 2104359 (2021).

34 Zinger, O. *et al.* Time-dependent morphology and adhesion of osteoblastic cells on titanium model surfaces featuring scale-resolved topography. *Biomaterials* **25**, 2695-2711 (2004).

35 Le Guehennec, L. *et al.* Osteoblastic cell behaviour on different titanium implant surfaces. *Acta biomaterialia* **4**, 535-543 (2008).

36 Chen, S. *et al.* Tuning surface properties of bone biomaterials to manipulate osteoblastic cell adhesion and the signaling pathways for the enhancement of early osseointegration. *Colloids and Surfaces B: Biointerfaces* **164**, 58-69 (2018).

37 Tolbert, C. E., Burridge, K. & Campbell, S. L. Vinculin regulation of F-actin bundle formation. *Cell Adhesion & Migration* **7**, 219-225, doi:10.4161/cam.23184 (2013).

38 Inman, C. K. & Shore, P. The osteoblast transcription factor Runx2 is expressed in mammary epithelial cells and mediates osteopontin expression. *Journal of Biological Chemistry* **278**, 48684-48689 (2003).

39 Komori, T. in *Osteoimmunology* 43-49 (Springer, 2009).

40 Vimalraj, S., Arumugam, B., Miranda, P. & Selvamurugan, N. Runx2: Structure, function, and phosphorylation in osteoblast differentiation. *International journal of biological macromolecules* **78**, 202-208 (2015).

41 Sladkova-Faure, M. *et al.* A biomimetic engineered bone platform for advanced testing of prosthetic implants. *Scientific Reports* **10**, 22154, doi:10.1038/s41598-020-78416-w (2020).

42 Cellini, F., Gao, Y. & Riedo, E. Å-Indentation for non-destructive elastic moduli measurements of supported ultra-hard ultra-thin films and nanostructures. *Scientific reports* **9**, 1-16 (2019).

43 Butt, H.-J. & Jaschke, M. Calculation of thermal noise in atomic force microscopy. *Nanotechnology* **6**, 1 (1995).

44 Paull, D. *et al.* Automated, high-throughput derivation, characterization and differentiation of induced pluripotent stem cells. *Nature Methods* **12**, 885-892, doi:10.1038/nmeth.3507 (2015).

5. Figures

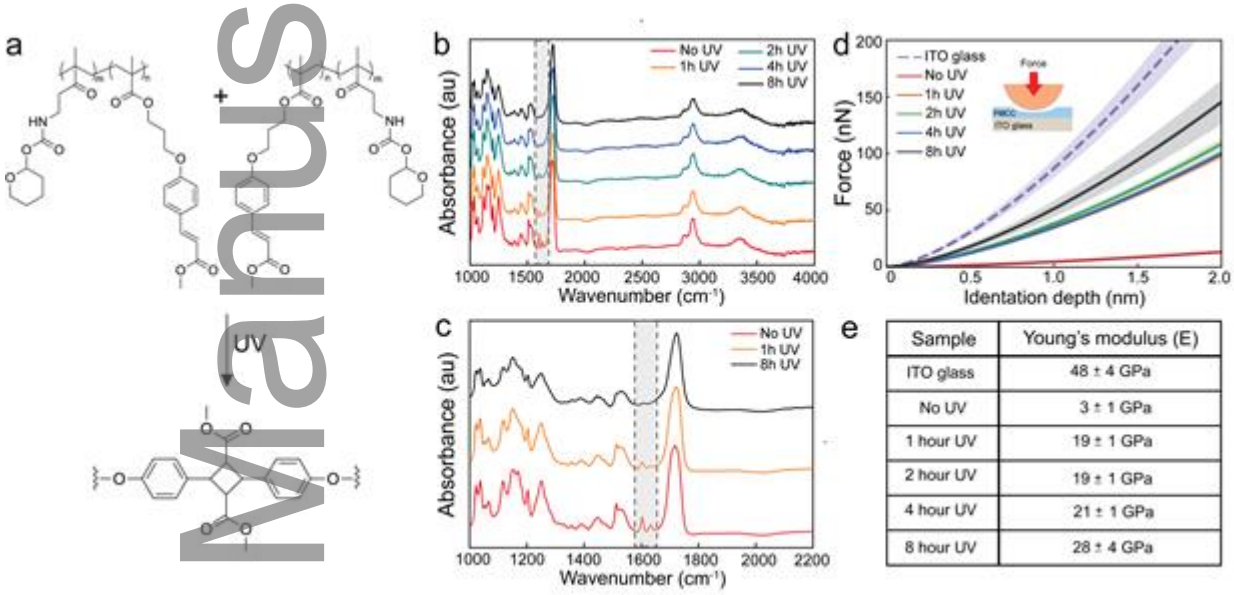

Sample	Young's modulus (E)
ITO glass	48 ± 4 GPa
No UV	3 ± 1 GPa
1 hour UV	19 ± 1 GPa
2 hour UV	19 ± 1 GPa
4 hour UV	21 ± 1 GPa
8 hour UV	28 ± 4 GPa

Figure 1. Tuning PMCC polymer stiffness by UV light. **(a)** Chemical structure of the PMCC resist before and after UV treatment showing the cross-linking of the cinnamate groups. **(b)** FTIR spectra of untreated PMCC films untreated and exposed to UV light (245 nm) for 1, 2, 4, and 8 hours. **(c)** Magnified FTIR spectra of PMCC films untreated and treated with UV light for 0, 1, and 8 hours showing the disappearance of the peaks associated with the double bond stretching mode in the cinnamate (~1600 cm^{-1}). **(d)** Experimental AFM indentation curves of glass substrate and PMCC film spin coated on ITO-glass substrates and exposed to UV light (245 nm) for 1, 2, 4, and 8 hours. **(e)** Values of PMCC film thickness after different UV exposure times and corresponding Young's modulus calculated from AFM indentation curves.

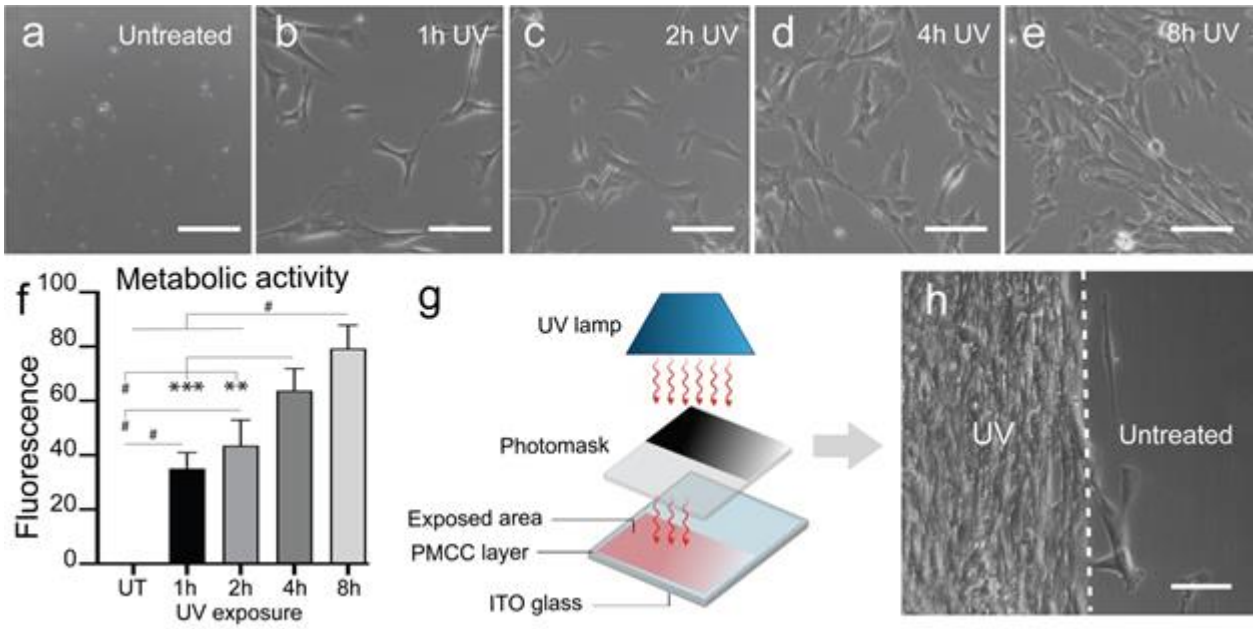

Figure 2. Cell attachment and growth on the PMCC films. Light micrographs of human iMSCs attached to PMCC-coated samples **(a)** not treated and **(b-e)** treated with UV light (245 nm) for 1, 2. 4, and 8 hours. **(f)** Metabolic activity of human iMSCs growing on the untreated PMCC films exposed and not exposed to UV light 5 days after seeding**.** Data are presented as mean ± standard deviation. Significance was calculated via one-way ANOVA with a Tukey *post-hoc* test (**P*<0.05, ***P*<0.01, #*P*<0.0001). **(g)** Schematic representation of UV patterning strategy to selectively increase stiffness on PMCC films. **(h)** Human iMSCs growing on a PMCC film patterned by UV light showing the ability to switch on/off cell attachment and growth by solely tuning the stiffness of the interface. Scale bar 100 µm.

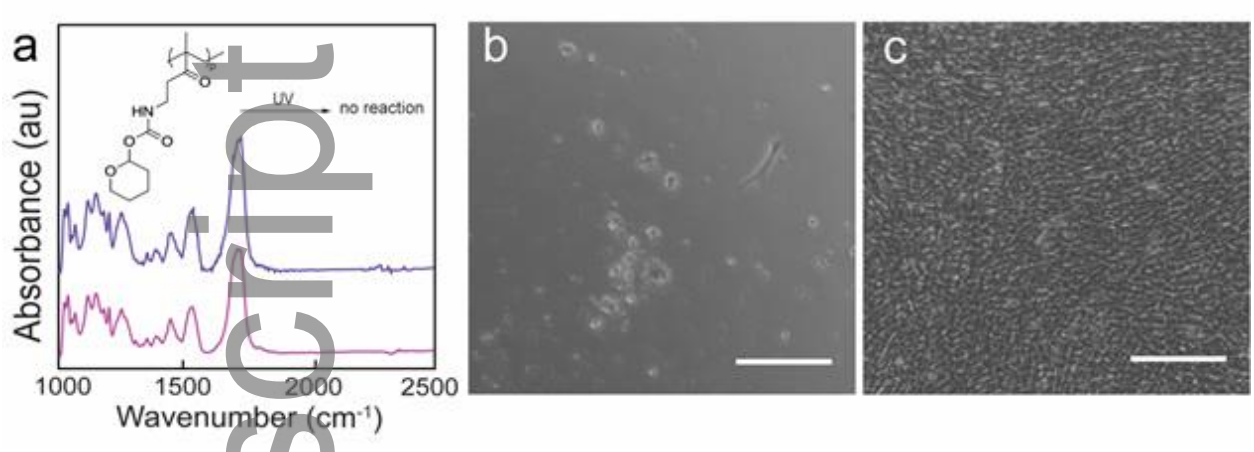

Figure 3. Characterization of PMCC films with and without the cinnamate moieties. (a) FTIR spectra of PMCC films without cinnamates before (pink line) and after (purple line) 1 hour of UV treatment (245 nm). **(b)** Micrographs showing human iMSCs after 10 days of culture on the PMCC films without and **(c)** with (right) the cinnamate moieties. Scale bar 250 µm.

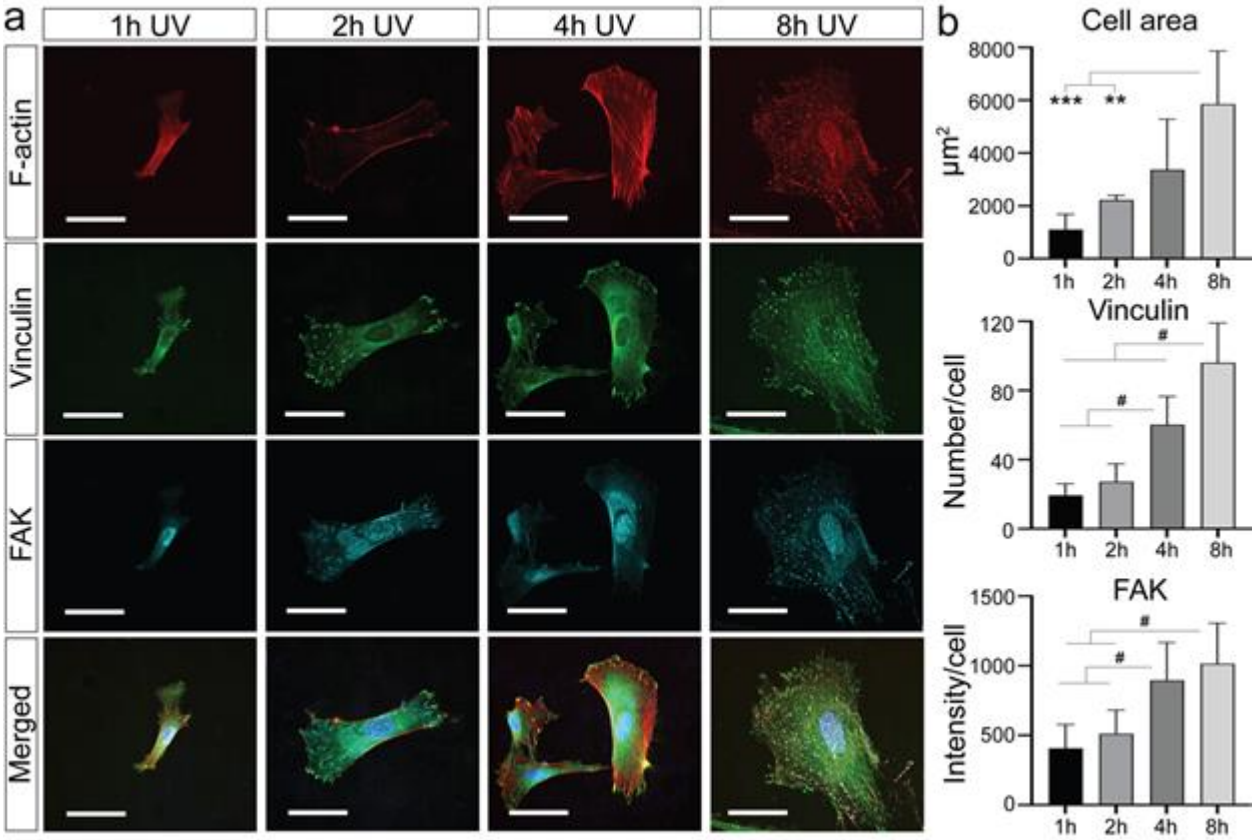

Figure 4. Cell size, morphology, and adhesion molecules. (a) Representative confocal images of human iMSCs cultured on UV-treated PMCC films and stained for F-actin, vinculin, and FAK (n = 20). Scale bar = 50μm. (b) Graphs showing the quantification of confocal images for F-actin (as an index of cell size), number of vinculin patches, and FAK (n = 20). Data are presented as mean ± standard deviation. Significance was calculated via one-way ANOVA with a Tukey *post-hoc* test (***P<0.001, $^{\#}P$<0.0001).

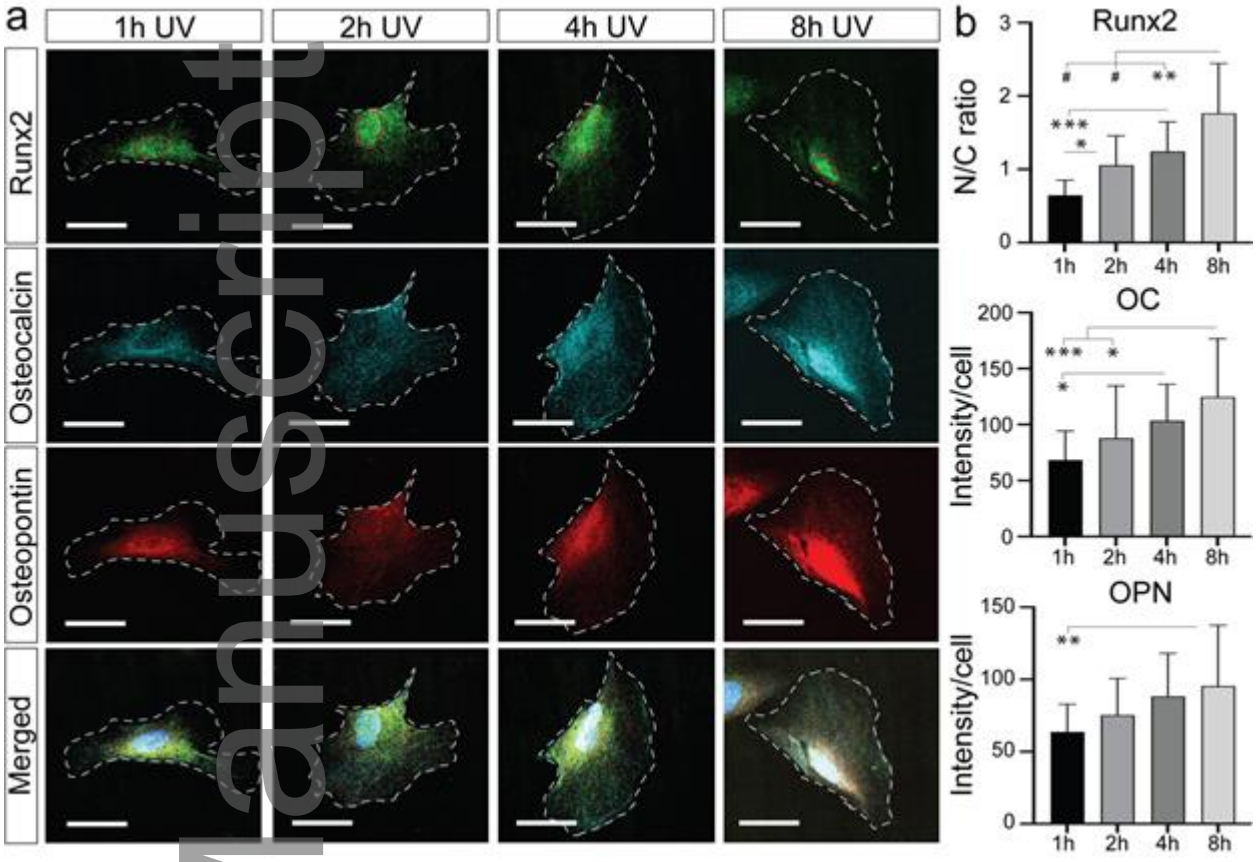

Figure 5. Osteogenic markers (a) Representative confocal images of human iMSCs cultured on UV-treated PMCC films and stained for the osteogenic markers runt-related transcription factor 2 (Runx2), osteocalcin (OC), and osteopontin (OPN) (n = 20). Cell boundaries are indicated by grey dashed circles, nuclei are indicated by blue dashed circles. Scale bar = 50µm. (b) Graphs showing the quantification of confocal images for all osteogenic biomarkers (n = 20) in the nuclei. Data are presented as mean ± standard deviation. Significance was calculated via one-way ANOVA with a Tukey *post-hoc* test (**P*<0.05, ***P*<0.01, ****P*<0.001, #*P*<0.0001).

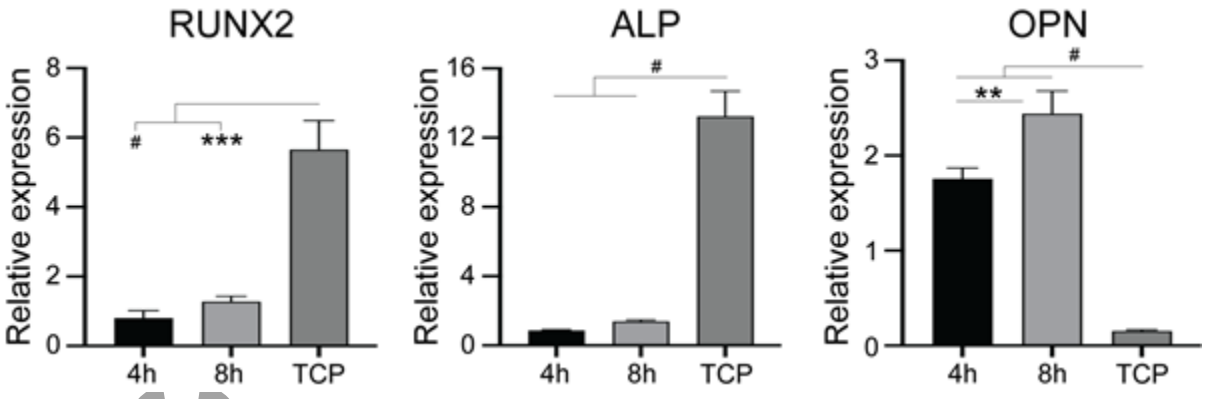

Figure 6. Osteogenic gene expression. Graphs showing the expression of runt-related transcription factor 2 (RUNX2), alkaline phosphatase (ALP), and osteopontin (OPN) in human iMSCs cultured on UV-treated PMCC films and tissue culture polystyrene (TCP) 2 weeks after treatment with osteogenic medium. Results are shown as normalized to the expression level of the housekeeping gene GAPDH. Data are presented as mean ± standard deviation. Significance was calculated via one-way ANOVA with a Tukey *post-hoc* test (***P*<0.01, ****P*<0.001, #*P*<0.0001).

Table of Contents

A novel platform to tune the stiffness of a biocompatible polymeric interface up to values characteristic of the bone tissue (GPa range) through UV cross-linking. Since cell growth and differentiation is controlled solely by UV treatment of the polymer, the platform is ideal for simple and rapid fabrication of stiffness patterns and gradients for various biomedical applications.

.